The Zinc Metalloregulatory Protein *Synechococcus* PCC7942 SmtB Binds a Single Zinc Ion per Monomer with High Affinity in a Tetrahedral Coordination Geometry†

Michael L. VanZile,‡ Nathaniel J. Cosper,§ Robert A. Scott,§ and David P. Giedroc*,‡

Department of Biochemistry and Biophysics, Center for Advanced Biomolecular Research, Texas A&M University, College Station, Texas 77843-2128, and Department of Chemistry, University of Georgia, Athens, Georgia 30602-2556

Received May 19, 2000

ABSTRACT: The *Synechococcus* PCC7942 SmtB is a zinc-responsive transcriptional repressor and a member of the ArsR superfamily of prokaryotic metalloregulatory transcription factors. The mechanism of negative regulation by Zn(II) and other metals as well as the coordination chemistry (stoichiometry, affinity, and specificity) of SmtB is poorly understood. In contrast to previous results [Kar, S. R., Adams, A. C., Lebowitz, J., Taylor, K. B., and Hall, L. M. (1997) *Biochemistry 36*, 15343−15348], we find that fully reduced SmtB binds 1 mol equiv of Zn(II) with a very high affinity, K_{Zn} in excess of 10^{11} M^{-1} (pH 7.4, 0.15 M KCl, 22 °C). Optical spectroscopic experiments reveal that SmtB binds 1 mol equiv of Co(II) in a tetrahedral or distorted tetrahedral environment with one or two cysteine thiolate ligands in the first coordination shell. Zn(II) and Co(II) EXAFS studies are consistent with the optical spectroscopic data, and further suggest the presence of a mixture of carboxylate and imidazole-containing ligands. K_{Co} was determined to be 1.7 (±0.1) × 10^9 M^{-1} in a chelator (EGTA) competition assay; 1 equiv of Zn(II) results in complete displacement of the bound Co(II). SmtB also binds 1 mol equiv of Ni(II), which, when formed at low Ni(II):SmtB molar ratios, adopts a non-native, six-coordinate complex characterized by at least two histidine and no thiolate ligands. The hierarchy of metal binding affinities is Zn(II) ≫ Co(II) ≫ Ni(II).

Metal ions are involved in many biological processes, serving as structural components of proteins or as cofactors in enzyme-catalyzed reactions (*1*, *2*). Metal-responsive control of the expression of genes involved in metal metabolism and metal homeostasis allows an organism to tightly regulate the free concentration of beneficial metal ions such as zinc, copper, and iron, while efficiently removing nonbeneficial or toxic metals (*3*, *4*). For example, a large class of evolutionarily related prokaryotic metalloregulatory repressor proteins (*5*) negatively regulate the expression of genes encoding intracellular metal chelators or metal efflux pumps.

The *smt* operon of *Synechococcus* PCC7942 and related strains contains two divergently transcribed genes, *smtA* and *smtB*, which play roles in the cellular response to excess zinc (for a review, see ref *6*). The *smtA* gene product is a ∼6.5 kDa class II metallothionein that functions in the sequestration and metabolism of zinc in *Synechococcus* (*7*). *SmtA* transcription is repressed in the absence of heavy metals and is derepressed in response to increased levels of Zn(II), Cd(II), and Cu(II), and, to a lesser extent, Co(II) and Ni(II) (*8*). SmtB is a dimeric trans-acting repressor that regulates the transcription of the *smtA* gene.

DNA methylation protection experiments suggest that there are two independent SmtB binding sites within the *smt* operon (*9*). One site overlaps the transcriptional start site for *smtA* and contains a pair of half-sites which together define an imperfect 12-2-12 inverted repeat. Each half-site is characterized by a consensus 5′-TGAA sequence to which SmtB binds (*9*). Although a second proposed SmtB binding site lies between the −10 boxes of the two *smt* genes (*9*), limited functional and electrophoretic mobility shift data suggest that SmtB in crude nuclear extracts binds to the site near the transcriptional start site for *smtA* (*10*) and mediates Zn(II)-dependent modulation of transcription (*6*). The highly related *Synechocystis* PCC6803 strain contains a homologous 12-2-12 inverted repeat near the transcription start site for *ziaA* which encodes a zinc efflux pump. Zn(II)-dependent transcriptional regulation of *ziaA* appears to require the binding of the SmtB homologue, ZiaR, to this 12-2-12 repeat (*11*).

The stoichiometry of the binding of SmtB to the *smt* operator/promoter region is unclear. Electrophoretic mobility shift assays seem to suggest that SmtB forms three resolvable complexes on an oligonucleotide containing the *smt* operator/promoter region (*9*, *10*). Formation of all three protein−DNA complexes has been reported to be strongly inhibited by the addition of Zn(II) ions in vitro to a total concentration in the 50−100 μM range (*9*). Consistent with this, SmtB has been reported to directly bind two Zn(II) ions per monomer with an affinity K_{Zn} of 3 × 10^5 M^{-1} as determined by equilibrium dialysis (*12*).

SmtB is a member of the ArsR family of metalloregulatory proteins which includes ZiaR, as well as the founding

† This work was supported by NIH Grants GM42569 (D.P.G.) and GM42015 (R.A.S.) and the Robert A. Welch Foundation (A-1295 to D.P.G.). M.L.V. was supported by NIH Chemistry−Biology Interface Training Grant T32-GM08523, and N.J.C. was supported by an NSF Research Training Group Award in Prokaryotic Diversity (BIR-9143235).

* To whom correspondence should be addressed. Telephone: 979-845-4231. FAX: 979-862-4718. E-mail: giedroc@tamu.edu.

‡ Texas A&M University.

§ University of Georgia.

10.1021/bi001140o CCC: $19.00
Published on Web 08/30/2000

member, ArsR, and *S. aureus* CadC, which regulate the expression of metal efflux pumps involved in arsenical and cadmium/lead resistance, respectively (*13*). The X-ray crystallographic structure of metal-free SmtB reveals a 2-fold symmetric, largely α-helical dimer in which two monomers interact mainly through their C-terminal α-helices. Mercuric acetate soaks of these crystals reveal that each monomer of the SmtB contains two Hg(II) binding sites. One site is formed by the side chains of Cys61, Asp64, and His97, while the other site is formed by two pairs of amino acid residues: a pair derived from each monomer, at the dimer interface (Asp104 and His106 from one monomer with His117′ and Glu120′ derived from the other) (*14*). The structural and functional significance of these putative metal sites is unclear due to questions concerning metal site occupancy, the rather unusual coordination geometries, and the long metal−ligand bond lengths observed in these complexes. However, site-directed mutagenesis has implicated His105 and/or His106 as divalent metal ion ligands which may be important for Zn(II) sensing in vivo (*15*). The His residue in *Synechocystis* ZiaR analogous to His106 in SmtB is also required for Zn(II) regulation in that system, as is one of two cysteines, Cys71 (analogous to SmtB Cys61) or Cys73 (*11*). His106 lies at the dimer interface formed by the C-terminal α-helices of each monomer, far removed from the putative DNA binding domain. Of the three cysteine residues of SmtB, only Cys14, in an N-terminal region (residues 1−21) that is not observed crystallographically (*14*), has been proposed to play a role in metal coordination and sensing as suggested by a reduced Zn(II) responsiveness relative to wild-type SmtB in vivo (*15*) and by preliminary NMR experiments (*16*).

As summarized above, the coordination chemistry and geometry of the native metal site(s) in *Synechococcus* SmtB and the mechanism of allosteric regulation of DNA binding by metal ions remain poorly understood. This is true for all members of the ArsR family of metalloregulatory repressors. In contrast to the previous report (*12*), we present evidence here which shows that SmtB contains a single high-affinity binding site for Zn(II) ($K_{Zn} \geq 10^{11}$ M^{-1}). Zn(II) EXAFS[1] of this site is most consistent with the presence of one cysteine sulfur ligand and three lighter (N,O) atoms, including at least one carboxylate ligand. Consistent with this, when the Zn(II) is substituted with Co(II), the UV−visible spectrum is characteristic of a coordination complex conforming to tetrahedral or distorted tetrahedral symmetry, with one or two thiolate ligands. Co(II) binds tightly, with a $K_{Co} = 1.7$ (± 0.1) $\times 10^9$ M^{-1}. The relative magnitudes of K_{Zn} and K_{Co} for tetrahedrally bound Zn(II) and Co(II), respectively, are consistent with one another (*17*). Ni(II) also forms a 1:1 complex with each SmtB monomer, with UV−visible absorption and Ni XAS spectra that are consistent with a non-native six-coordinate complex containing two imidazole ligands. The hierarchy of metal affinities is Zn(II) ≫ Co(II) ≫ Ni(II). The implications of these findings for the mechanism of metalloregulation by SmtB and related metalloregulatory repressors are discussed.

[1] Abbreviations: DTNB, 5,5′-dithiobis(2-nitrobenzoic acid); EDTA, ethylenediaminetetraacetic acid; EGTA, ethylene glycol bis(β-aminoethyl ether)-*N*,*N*,*N*′,*N*′-tetraacetic acid; EXAFS, extended X-ray absorption fine structure; FT, Fourier transform; HEPES, *N*-(2-hydroxyethyl)-piperazine-*N*′-2-ethanesulfonic acid; IPTG, isopropyl β-D-thiogalactopyranoside; MES, 2-(*N*-morpholino)ethanesulfonic acid; PAR, 4-(2-pyridylazo)resorcinol; NTA, nitrilotriacetic acid; PMSF, phenylmethylsulfonyl chloride; Tris, tris(hydroxymethyl)aminomethane; XAS, X-ray absorption spectroscopy.

MATERIALS AND METHODS

Chemicals. All buffers were prepared using Milli-Q deionized water. MES, HEPES, and Tris buffer salts and ammonium sulfate were obtained from Sigma. All chromatography materials were obtained from Pharmacia Biotech. Ultrapure cobalt(II) chloride and zinc sulfate were obtained from Johnson-Matthey. The indicators mag-fura-2 and 4-(2-pyridylazo)resorcinol (PAR) were purchased from Molecular Probes and Kodak, respectively. The SmtB overexpression plasmid pSRK15-1 was generously provided by Dr. L. Hall at the University of Alabama−Birmingham.

Growth of BL21(DE3)/pSRK15-1. Expression of SmtB in *E. coli* BL21(DE3)/pSRK15-1 was carried out by preparing a seed culture in LB containing 60 mg/L kanamycin sulfate at 37 °C from a fresh colony grown at 37 °C on a 1.5% agar plate of the same medium. A 9 mL aliquot was used to inoculate 9 L of the same culture medium. The cells were grown at 37 °C with stirring (300 rpm) to an OD of 0.6−0.8 at 600 nm in a New Brunswick Scientific Series 25 incubator/shaker. SmtB expression was induced by the addition of IPTG to a concentration of 400 μM. Cells were collected by centrifugation to yield 20−25 g of wet cell paste which was either used immediately or stored at −20 °C overnight.

Purification of SmtB. SmtB purification was carried out with a variation of the procedure described by (*12*). Forty-five grams of cell paste was slurried in a 1:5 (w/v) mixture of buffer B (25 mM MES, 2 mM DTT, 2 mM EDTA, pH 6.0) containing 200 μL of PMSF (0.1 M) and lysed at 20 000 psi by French press. The cellular lysate was centrifuged at 8000 rpm for 30 min at 4 °C. The supernatant and a gelatinous zone near the packed precipitate were collected. Precipitation of protein and nucleic acid was accomplished by dropwise addition of a 10% polyethylenimine solution (0.015 v/v) at pH 6.0. After stirring for 2 h, the solution was centrifuged at 8000 rpm for 30 min, and the precipitate was retained. Protein was extracted from the precipitate by stirring for 8 h in a solution of 0.5 M NaCl in buffer B (5 mL/g of cell paste). After centrifugation at 8000 rpm for 30 min, the protein in the supernatant was precipitated by the addition of solid $(NH_4)_2SO_4$ to 3.0 M with stirring for 2 h. The precipitate was collected by centrifugation at 12 000 rpm for 30 min and dissolved in 200 mL of buffer B. The resuspended protein was then loaded onto a 50 mL SP Fast Flow gravity column that had been equilibrated with buffer B. After sample application, the column was washed with 50 mL of 0.25 M NaCl in buffer B, and SmtB was eluted with a 150 mL linear gradient of 0.25−1.0 M NaCl in buffer B. SmtB eluted at approximately 0.6 M NaCl. Fractions containing SmtB were combined (40 mL) and concentrated to 8−10 mL using a 50 mL Amicon concentrator equipped with a YM3 membrane. The concentrated sample was then loaded onto a 100 mL Superdex 75 size-exclusion column at 0.4 mL/min. SmtB was eluted by washing the column with 0.5 M NaCl in buffer B at 0.4 mL/min. Fractions containing SmtB were combined (10 mL) and diluted 1:10 with buffer E (25 mM Tris, 2 mM DTT, 2 mM EDTA, pH 8.0) prior to loading onto a 50 mL Q Fast Flow gravity

column. After sample loading, the column was washed with 50 mL of buffer E, and SmtB was eluted with a linear gradient of 0−0.5 M NaCl in buffer E. SmtB eluted at ~0.3 M NaCl, and fractions were combined (20 mL). The purified SmtB was then dialyzed against 5 L of buffer S* (10 mM HEPES, 2 mM DTT, 2 mM EDTA, 0.15 M KCl, pH 7.4) with changes every 4 h for a total of 36 h of dialysis. All of the above purification steps were carried out at 4 °C. The freshly dialyzed SmtB was then dialyzed against 3 L of buffer S (10 mM HEPES, 0.15 M KCl, pH 7.4) in an anaerobic Vacuum Atmospheres glovebox with changes every 2 h for a total of 8 h at room temperature. The purity of SmtB prepared in this way was estimated by inspection of overloaded Coomassie-stained gels to be ≥95%. Purified SmtB was stored at −80 °C in an anaerobic environment. The concentration of purified SmtB was determined using the calculated molar extinction coefficient at 280 nm of 5960 M^{-1} cm^{-1} (*18*).

Atomic Absorption Spectrophotometry. The Zn(II) content of SmtB was determined using a Perkin-Elmer model 2380 atomic absorption spectrophotometer in flame mode with detection at 214 nm (slit = 0.7 nm). The zinc content of "metal free" SmtB used for metal titrations was found to range from 0.05 to 0.2 mol of Zn(II) per mole of SmtB monomer, with preparations purified in the absence of EDTA always higher. The Zn(II) concentration of the titrant used for the optical titration experiments was measured in the same way. The Co(II) concentration in the titrant was measured using a cobalt hollow cathode lamp (Perkin-Elmer) with detection set at 240.7 nm (slit = 0.2 nm).

Free Thiol Quantitation. The number of free thiols in SmtB was determined using a standard DTNB colorimetric assay (*17*). Protein samples were diluted to 20−40 μM in 400 μL of buffer S, and 25 μL of 2.5 mM DTNB solution was added. The reactions were incubated for 30 min in an anaerobic chamber before analysis to ensure that the reaction was complete. The reaction of DTNB with protein was monitored by recording the UV−visible spectrum from 240 to 600 nm. The molar concentration of liberated thiolate anion was quantified at 412 nm (ϵ = 13 600 M^{-1} cm^{-1}) after subtraction of the absorbance obtained from buffer alone. This determination allowed for the calculation of the free thiols in the protein. As purified, all preparations of SmtB contained 2.8−3.2 free thiols per monomer (expected number is 3).

Co(II) Binding Experiments. All metal binding experiments were carried out in buffer S at ambient temperature using a Hewlett-Packard model 8452A spectrophotometer. Apo SmtB (0.8 mL of 50−250 μM) was prepared by dilution with buffer S and loaded in an anaerobic cuvette; 250 μL of Co(II) titrant was taken up into an adjustable volume Hamilton syringe, and the syringe was attached to the cuvette to create an O_2-free sealed environment prior to removal from the glovebox. Optical spectra of the apoprotein and following each *i*th addition of a known aliquot of Co(II) titrant (5−20 μL) were collected from 190 to 1100 nm. Corrected spectra were obtained by subtraction of the apoprotein spectrum and correction for dilution. Titration experiments to determine K_{Co} were done in exactly the same way except that 1.0 mM EGTA was present to buffer very low concentrations of free Co(II), with K_{Co} determined essentially as described previously (*17*). The conditional stability of the Co(II)−EGTA complex was calculated to be 4.64 × 10^8 M^{-1} under these solution conditions using methods outlined in Fahrni and O'Halloran (*19*). Some experiments were done under aerobic conditions with no change in the metal binding isotherms or the concentration of reduced SmtB competent to bind metals. Equilibrium was shown to be established within 1.5−2 min after addition of metal.

Zn(II) Binding Experiments. Since Zn(II) is spectroscopically silent, three different methods were employed to investigate Zn(II) binding to SmtB. The first method involves a competition [Zn(II) vs Co(II)] experiment to determine if the Co(II) binding site was the same site for Zn(II). Apoprotein was titrated with Co(II), as described, to a stoichiometric excess [3−5 molar excess of Co(II)]. Optical spectra were then measured for each *i*th addition of $ZnSO_4$ titrant delivered from an adjustable volume Hamilton syringe. Spectra were corrected as described for the Co(II) binding experiments.

Mag-fura-2 was employed as a direct measurement of Zn(II) binding with SmtB via a competition experiment. A 16−20 μM sample of metal-free mag-fura-2, quantified from ϵ_{366} = 29 900 M^{-1} cm^{-1} (*20*), was mixed with apoprotein (10−60 μM) in 0.8 mL of buffer S and was denoted the "apo spectrum". Following each *i*th addition of $ZnSO_4$ (2.5−10 μL), the optical spectrum was recorded from 240 to 800 nm. Spectra were corrected as described for the Co(II) experiments. Since Zn(II) binding to mag-fura-2 results in a shift from an absorption maximum of 366 nm to 325 nm, it was possible to determine the concentration at which Zn(II) begins to bind to mag-fura-2. In this way, the stoichiometry of Zn(II) binding to SmtB and the relative affinity of SmtB for Zn(II) could be inferred.

4-(2-Pyridylazo)resorcinol (PAR) was also employed in a competition assay with SmtB (*20*, *21*). A known concentration of PAR (200−400 μM) was mixed with $ZnSO_4$ (10−20 μM) and the optical spectrum recorded. Following each *i*th addition of SmtB (typically 2.5 μL of a concentrated stock solution), the spectrum was recorded and corrected by subtraction of the "apo-spectrum" and dilution. In this manner, it was possible to determine the concentration of SmtB required to induce complete dissociation of the PAR_2−Zn complex.

Ni(II) Binding Experiments. Ni(II) binding experiments were carried out in exactly the same way as the Co(II) binding experiments, except that these were done under aerobic conditions. The total SmtB concentration was varied from 22 to 198 μM in multiple experiments.

X-ray Absorption Spectroscopy. These samples were prepared in polycarbonate XAS cuvettes and were immediately frozen in liquid N_2 to exclude oxygen. Samples typically contained 1.0 mM SmtB to which 0.8 molar equiv of metal per monomer SmtB was added in 10 mM HEPES, 0.15 M KCl, 20% v/v glycerol, pH 7.4. XAS data were collected at 10 K according to standard procedures (*22*) at the Stanford Synchrotron Radiation Laboratory, beam-line 7-3, with the SPEAR storage ring operating in a dedicated mode at 3.0 GeV (Table 1). Data reduction and analysis were performed using EXAFSPAK software (www-ssrl.slac.Stanford.edu/exafspak.html), as described previously (*23*, *24*). Multiple scattering models, calculated using FEFF version 7.02 (*25*), were based on bis(aceto)-bis(imidazole)zinc(II) (*26*), tetra(imidazole)-zinc(II) (*27*), hexakis(imidazole)nickel-

Table 1: X-ray Absorption Spectroscopic Data Collection for Zn, Ni, and Co Analysis

	Zn EXAFS	Ni EXAFS	Co EXAFS
SR facility	SSRL	SSRL	SSRL
beamline	7-3	7-3	7-3
current in storage ring, mA	50−100	50−100	50−100
monochromator crystal	Si[220]	Si[220]	Si[220]
detection method	fluorescence	fluorescence	fluorescence
detector type	solid state array[a]	solid state array	solid state array
scan length, min	25	25	25
scans in average	10	8	15
temperature, K	10	10	10
energy standard	Zn foil, first inflection	Ni foil, first inflection	Co foil, first inflection
energy calibration, eV	9660.7	8331.6	7709.5
E_0, eV	9670	8340	7715
preedge background			
energy range, eV	8657−9625	8008−8295	7385−7670
Gaussian center, eV	8638	7477	6930
width, eV	750	985	925
spline background			
energy range, eV	9670−9902 (4)	8340−8543 (4)	7715−7950 (4)
(polynomial order)	9902−10134 (4)	8543−8746 (4)	7950−8184 (4)
	10134−10366 (4)	8746−8950 (4)	8184−8419 (4)

[a] The 13-element Ge solid-state X-ray fluorescence detector at SSRL is provided by the NIH Biotechnology Research Resource.

(II) chloride tetrahydrate (*28*), or hexakis(imidazole)cobalt-(II) carbonate pentahydrate (*29*).

RESULTS

Co(II) Titrations of SmtB. Shown in Figure 1A are UV−visible absorption spectra which result upon anaerobic titration of metal-free apo-SmtB with Co(II) (pH 7.4, 0.15 M KCl, 22 °C). The intense absorption bands present in the near-ultraviolet at 315 and 365 nm are indicative of $S^- \rightarrow$Co(II) ligand-to-metal charge-transfer absorption (*30*, *31*). The absolute magnitude of the molar absorption (ϵ) at ≈320 nm reports on the number of thiolate groups coordinated to the metal, and averages ≈900−1200 M^{-1} cm^{-1} per S^-−Co(II) bond (*32*, *33*). In SmtB, ϵ_{320} is ≈1500 M^{-1} cm^{-1} and is therefore most consistent with the presence of one, or perhaps two, thiolate ligands in the first coordination sphere of the bound Co(II). Further support for this comes from the energies of the $^4A_2 \rightarrow {}^4T_1$(P) d−d electronic transition envelope, which in Co(II)-SmtB is centered around 550 nm. Previous studies of Co(II)-substituted zinc metalloproteins reveal that as the number of Co(II)−thiolate bonds increases in a tetrahedral complex, this d−d ligand field envelope moves to increasingly lower energies, and often gains molar absorptivity (*17*, *34*, *35*). The ligand field envelope for Co(II)-SmtB is somewhat more blue-shifted than other complexes containing two Co(II)−sulfur bonds (*17*, *36*), and thus may be more consistent with one cysteine thiolate ligand. In any case, the molar intensity of the ligand field envelope [ϵ_{593} = 570 (±20) M^{-1} cm^{-1}] is consistent with Co(II) bound in a tetrahedral or distorted tetrahedral coordination geometry. The inset to Figure 1A shows a binding isotherm generated from the titration data [ϵ_{593} vs Co(II):SmtB monomer ratio] that shows that Co(II) and SmtB form a stoichiometric 1:1 Co(II)/SmtB monomer complex. K_{Co} cannot be estimated from this binding isotherm since the binding of Co(II) is essentially stoichiometric under these conditions.

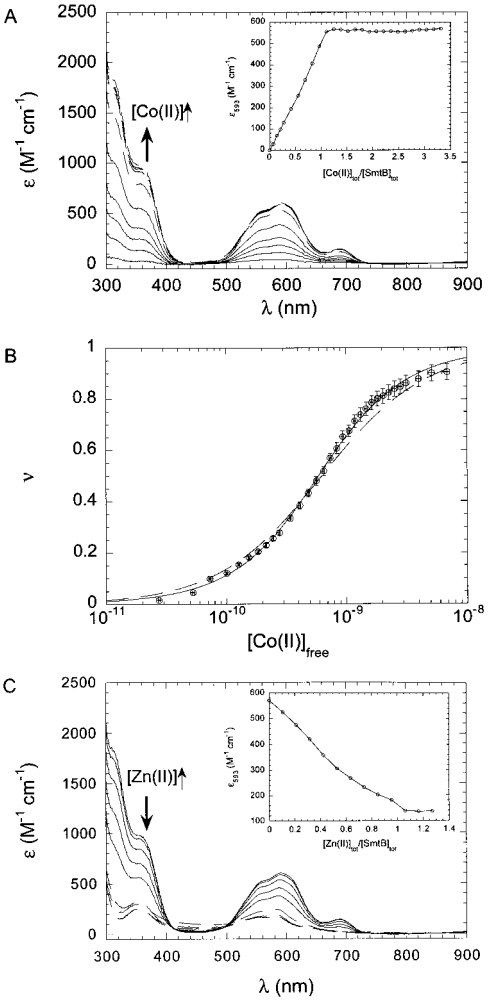

FIGURE 1: Co(II) titrations of SmtB and subsequent displacement by added Zn(II). (A) Optical absorption spectra of SmtB anaerobically titrated with increasing concentrations of Co(II). Inset: Co(II) binding isotherm generated from the optical spectra is plotted as ϵ_{593} vs total [Co(II)]/total SmtB monomer ratio. (B) Representative Co(II) binding isotherm obtained for 98 μM SmtB in the presence of 1.0 mM EGTA (see Materials and Methods for details). ν was calculated from A_{593} using ϵ_{593} = 570 (±20) M^{-1} cm^{-1} derived from multiple determinations such as that shown in panel A. The dashed curve represents a nonlinear least-squares fit to a 1:1 binding model with $K_{Co} = 1.7\ (\pm 0.1) \times 10^9\ M^{-1}$. The solid curve is a fit to a two-site cooperative binding model with $K_{int} = 1.1\ (\pm 0.1) \times 10^9\ M^{-1}$ and $\omega = 2.3\ (\pm 0.2)$ (see text for details). Here, macroscopic $K_1 = 2{*}K_{int}$ and macroscopic $K_2 = K_{int}{}^{2}{*}\omega$, where $\sqrt{K_2}$ is analogous to K_{Co} from the 1:1 binding model analysis. From these data, $\sqrt{K_2} = 1.7 \times 10^9\ M^{-1}$. (C) Optical absorption spectra of Co(II)-substituted SmtB in the presence of 4 molar equiv of Co(II) recorded after the addition of increasing amounts of Zn(II). Inset: Zn(II) displacement binding isotherm that results from analysis of the spectral data plotted as ϵ_{593} vs total [Zn(II)]/total SmtB monomer ratio. Conditions: pH 7.4, 0.15 M KCl, 22 °C.

One way to obtain a quantitative estimate of K_{Co} is to carry out Co(II) binding experiments such as those shown in Figure 1A under exactly the same solution conditions, except that an appropriate metal chelating agent is present in excess over protein concentration in order to buffer very low concentrations of free Co(II) (cf. ref *37*). We used 1.0 mM ethylene glycol bis(β-aminoethyl ether)-*N*,*N*,*N*′,*N*′-tetraacetic acid (EGTA) for this purpose (*17*). The results of a representative titration collected at 98 μM SmtB monomer are shown in

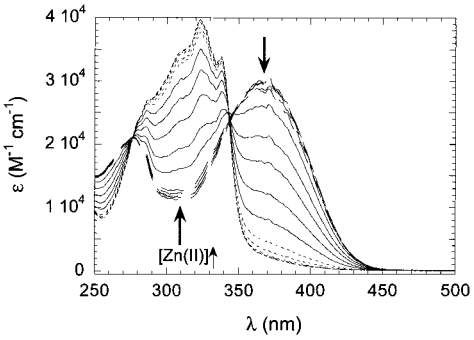

FIGURE 2: Representative titration of a ≈1:1 SmtB monomer/mag-fura-2 mixture with Zn(II). [SmtB monomer] = 21 μM; [mag-fura-2] = 17.5 μM. In all cases, the spectrum of apo-SmtB has been subtracted from the mag-fura-2 spectra. Arrows indicate the direction of the change in the absorption spectrum of mag-fura-2 as Zn(II) is bound by the dye. Conditions: pH 7.4, 0.15 M KCl, 22 °C.

Figure 1B. Using expressions outlined in (*17*), K_{Co} was determined to be 1.7 (±0.1) × 10^9 M^{-1} from two separate experiments. K_{Co} values resolved from competition experiments carried out in the presence of nitrilotriacetic acid (NTA) are within 2-fold of K_{Co} determined from EGTA titrations (data not shown). Interestingly, although this has no impact on our estimate of K_{Co}, both fitted isotherms systematically miss the experimental data slightly at both low and high free Co(II) in a way which cannot be accounted for by uncertainties in ϵ_{593} or [EGTA]. The origin of this is unknown but may be reporting on linkage to the SmtB monomer−dimer equilibrium (*12*) or modestly cooperative binding of two Co(II) ions to the dimeric form of SmtB. Estimates of the concentrations of SmtB monomer and dimer determined from the dimerization association equilibrium constant for the apoprotein reported under similar solution conditions (*12*) suggest that ≥90% of the SmtB is dimeric under these conditions; thus, strong linkage to the monomer−dimer equilibrium seems unlikely here. The solid line shows a best-fit to a cooperative binding model of Co(II) binding to two identical sites, one on each SmtB monomer, with the results from two independent experiments returning $\omega = 4.1$ (±2.1) and $K_{int,\ Co} = 8.7\ (\pm 1.5) \times 10^8\ M^{-1}$. Thus, we conclude that Co(II) binding to the SmtB dimer occurs with high affinity and is weakly or noncooperative.

Zn(II) Competition of Co(II) Binding to SmtB. Figure 1C shows the results of a titration of Co(II)-substituted SmtB with Zn(II). Complete diminution of the d−d ligand field transitions as well as the $S^- \rightarrow Co(II)$ charge-transfer bands occurs upon titration with Zn(II). The simplest interpretation of this experiment is that Zn(II) and Co(II) occupy the same binding site on SmtB. This suggests that the Zn(II) binding site geometry is tetrahedral and contains one thiolate ligand in the inner coordination sphere. The inset to Figure 1C reveals that 1 mol equiv of Zn(II) is required to displace all of the bound Co(II), even at a slight excess of Co(II). Such a competition experiment could not be carried out to estimate K_{Zn} (*17*) since the vast excess of Co(II) required by this experiment results in precipitation of the protein (data not shown). In any case, this experiment suggests that the relative affinity of SmtB for Zn(II) may well be greater than that for Co(II), which is expected since Zn(II) has been shown to derepress the transcription of the *smt* operon more effectively than Co(II) (*8*). This is also expected on the basis of ligand-field stabilization energy arguments for tetrahedral Zn(II) vs tetrahedral Co(II) (*38*).

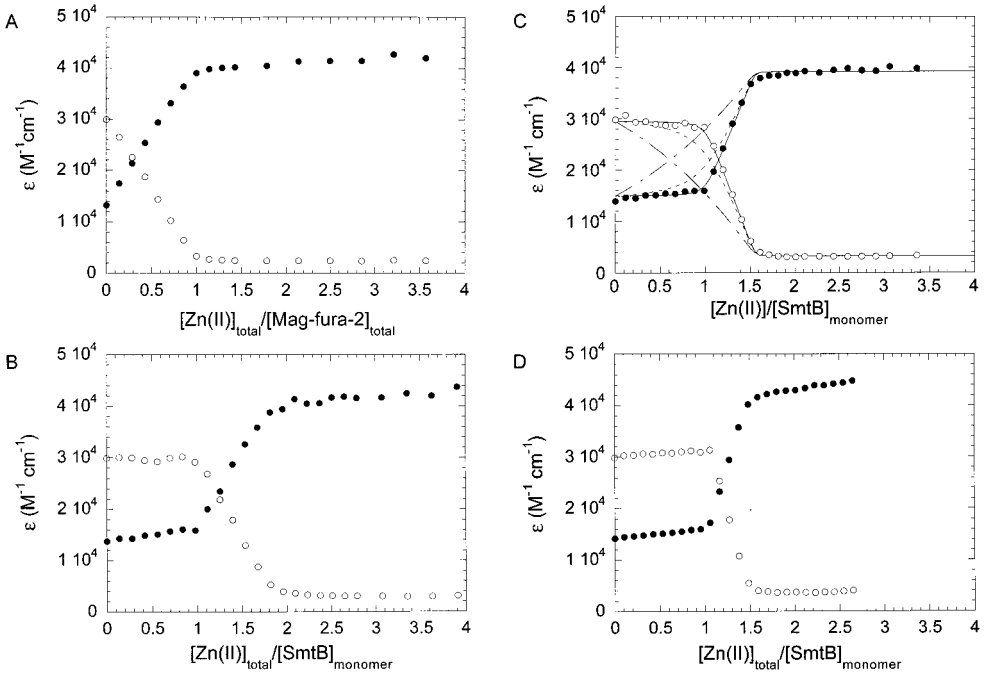

FIGURE 3: Zn(II) titrations of various SmtB/Mag-fura-2 ratios. (A) 0 μM SmtB, 17 μM mag-fura-2; (B) 21 μM SmtB and 17.5 μM mag-fura-2; (C) 31 μM SmtB and 17.3 μM mag-fura-2; and (D) 45 μM SmtB and 17.4 μM mag-fura-2. In all four panels, the closed circles represent ϵ_{325} [which is maximal in the Zn(II)−mag-fura-2 complex], and the open circles represent ϵ_{366} (which is maximal in apo mag-fura-2). In panel A, the changes in molar absorptivity are plotted as a function of the total Zn(II) to total mag-fura-2 ratio, while in panels B−D the data are plotted as a function of the total Zn(II) to total SmtB monomer ratio. In panel C, theoretical isotherms generated with the program DynaFit (*53*) are shown for K_{Zn} of 10^{10} M^{-1} (—), 10^9 M^{-1} (---), and 10^8 M^{-1} (— · —) superimposed on the experimental data. The solution conditions are identical to those in Figure 2.

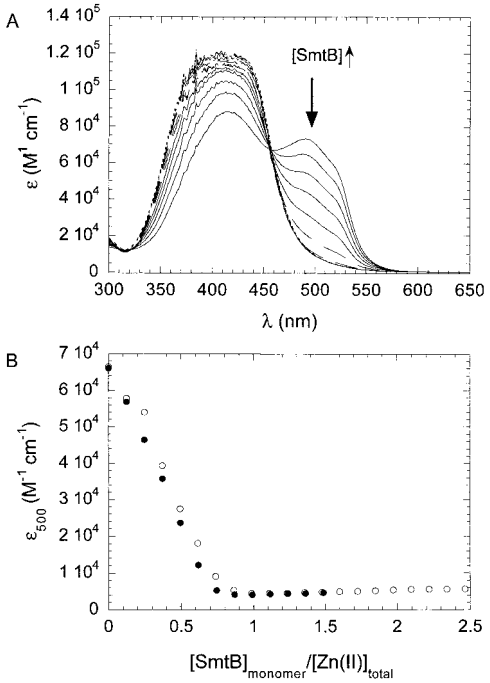

FIGURE 4: Titration of 200 μM PAR and 10 μM Zn(II) with increasing concentrations of SmtB dispensed from a 200 μM SmtB (monomer) stock solution. The preparation of SmtB used in this experiment contained 0.20 mol equiv of Zn(II). (A) Optical spectra recorded during the course of the titration. Reduction in ϵ_{500} is reporting on dissociation of the PAR_2-Zn complex by added apo-SmtB to form Zn(II)−SmtB. (B) Binding isotherm generated from the data collected in panel A. The open and closed circles represent the results obtained from two independent experiments. Conditions: pH 7.4, 0.15 M KCl, 22 °C.

Zn(II) Titration of SmtB in the Presence of Mag-Fura-2, a Zinc Indicator Dye. Since it was impossible to determine the affinity of SmtB for Zn(II) using a competition assay with Co(II)-SmtB due to the insolubility of SmtB at the high concentrations of Co(II) required by these experiments, the fluorescent indicator mag-fura-2 was employed (*20*). Mag-fura-2 is reported to form a 1:1 complex and binds Zn(II) with an affinity of 5×10^7 M^{-1} (pH 7.0, 25 °C). The binding of zinc to mag-fura-2 can be followed by monitoring the changes in the UV−vis absorption spectrum of the dye (Figure 2). When Zn(II) binds to mag-fura-2, there is a shift in the absorption maximum from 366 to 325 nm with a substantial decrease in the molar absorptivity at 366 nm (from 29 900 to 1880 M^{-1} cm^{-1}) (Figure 2). In contrast to observations in the absence of SmtB (Figure 3A), as Zn(II) is titrated into a solution containing both SmtB and mag-fura-2, there is essentially no change in the absorption spectrum of apo-mag-fura-2 until sufficient Zn(II) is added to saturate the single Zn(II) binding site on each SmtB monomer (Figure 3B−D). As the concentration of SmtB monomer is increased relative to mag-fura-2, it takes a correspondingly larger concentration of Zn(II) before significant Zn(II) begins binding to the indicator dye (Figure 3B−D). In all cases, the data indicate that the single binding site on each SmtB monomer must be fully occupied before the binding occurs to mag-fura-2. Unfortunately, since Zn(II) binds to SmtB so avidly in the presence of mag-fura-2, this experiment can only be used to set a lower limit to the affinity of SmtB for Zn(II) at $K_{Zn} > 10^{10}$ M^{-1} (see simulations in Figure 3C).

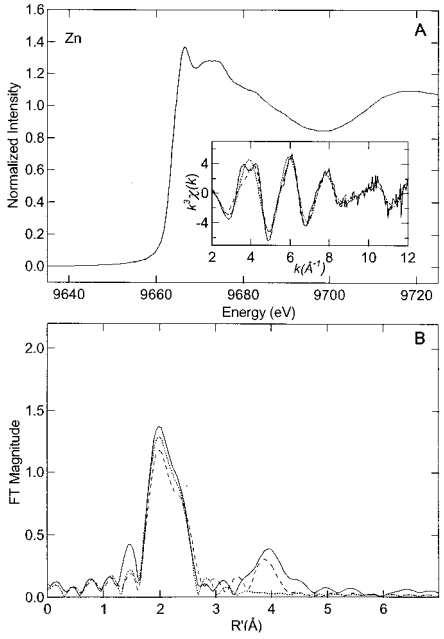

FIGURE 5: Zn K-edge X-ray absorption spectrum for Zn(II)−SmtB [1:1 Zn(II):SmtB monomer] (A) and k^3-weighted EXAFS (A, inset) and Fourier transforms (B; $k = 2-12$ $Å^{-1}$) for Zn(II)−SmtB (solid line) and theoretical EXAFS and FTs for $Zn-S(O,N)_3$ (dotted line; fit 1, Table 2) and $Zn-S(imid)_2(carboxylate)$ (dashed line; fit 3, Table 2).

SmtB Titrations of PAR_2-Zn. Under these solution conditions (pH 7.4), PAR is calculated to form 1:1 and 2:1 complexes with Zn(II) with stepwise affinity constants of 7.7×10^6 and 5.0×10^5 M^{-1}, respectively, which corresponds to an overall conditional stability constant (β') of 3.85×10^{12} M^{-2} (*39*). For this reason, an excess of PAR was used in our experiments to ensure that the PAR_2-Zn complex was the only Zn(II) complex in solution prior to addition of protein. PAR is a useful indicator since addition of Zn(II) results in an intense absorption band at 500 nm ($\Delta\epsilon = 66\,000$ M^{-1} cm^{-1}), and it is therefore capable of reporting on dissociation equilibrium constants of protein−zinc complexes in the nanomolar to picomolar range (*20, 21*). A representative titration of a PAR_2-Zn solution with SmtB is shown in Figure 4A. As is evident, the absorption spectrum of the PAR_2-Zn complex decreases as SmtB is titrated into solution. The binding isotherm shown in Figure 4B reveals that one SmtB monomer is required to quantitatively remove the Zn(II) from the PAR_2-Zn complex and that this removal occurs in a stoichiometric manner. Estimation of the $[SmtB]_{free}$ using methods previously described (*20, 21*) suggests that there is essentially no free SmtB in solution until the $[SmtB]_{total}$ is greater than the $[Zn]_{total}$. This experiment suggests a lower limit for K_{Zn} of 10^{11} M^{-1}. Consistent with this, a titration of Zn(II) into a solution containing 20 μM SmtB monomer and 200 μM PAR as outlined in Jefferson et al. (*21*) resolves K_{Zn} of 4.2 ($\pm$1.5) $\times$ 10^{11} M^{-1}, or approximately 250-fold large than K_{Co} (data not shown).

X-ray Absorption Spectroscopy. The intensities of the first two peaks in the Zn K-edge X-ray absorption spectrum (Figure 5A) of Zn-substituted SmtB and the position of the edge (9663.4 eV) are indicative of a Zn(II) site coordinated by a mixture of sulfur and light atoms (nitrogen or oxygen) (*40, 41*). The results of extensive curve fitting are most consistent with the interpretation that SmtB contains a first-

Table 2: Curve-Fitting Results for Zn EXAFS of SmtB[a]

sample filename (k range) $\Delta k^3\chi$	fit	shell[b]	R_{as} (Å)	σ_{as}^2 (Å^2)	f'[c]
wt SmtB+Zn	1	Zn−N_3	1.97	0.0036	0.075
P2Z2D (2−12 Å^{-1})		Zn−S	2.29	0.0026	
$\Delta k^3\chi = 11.71$					
	2	Zn−S	2.30	0.0016	0.071
		Zn−N_3	1.99	0.0020	
		Zn−C_2	2.97	0.0082	
		Zn−C_2	[3.03]	[0.0083]	
		Zn−C_2	[4.12]	[0.0113]	
		Zn−N_2	[4.16]	[0.0115]	
	3	Zn−S	2.31	0.0015	0.066
		Zn−N_2	2.02	0.0010	
		Zn−C_2	2.94	0.0003	
		Zn−C_2	[3.08]	[0.0005]	
		Zn−C_2	[4.11]	[0.0007]	
		Zn−N_2	[4.19]	[0.0007]	
		Zn−O	1.93	0.0018	
		Zn−C	[2.85]	[0.0027]	
		Zn−O	[3.12]	[0.0031]	

[a] Group is the chemical unit defined for the multiple scattering calculation. N_s is the number of scatterers (or groups) per metal. R_{as} is the metal-scatterer distance. σ_{as}^2 is a mean square deviation in R_{as}. ΔE_0 is the shift in E_0 for the theoretical scattering functions. Parameters in square brackets were constrained to be multiples of the value above. [b] Subscripts indicate the number of scatterers for that shell. For fit 2, there are three first-shell nitrogen scatterers and two imidazole ligands. [c] f' is a normalized error (chi-squared): $f' = \frac{\left\{\sum_i [k^3(\chi_i^{obs} - \chi_i^{calc})]^2/N\right\}^{1/2}}{[(k^3\chi^{obs})_{mzx} - (k^3\chi^{obs})_{min}]}$.

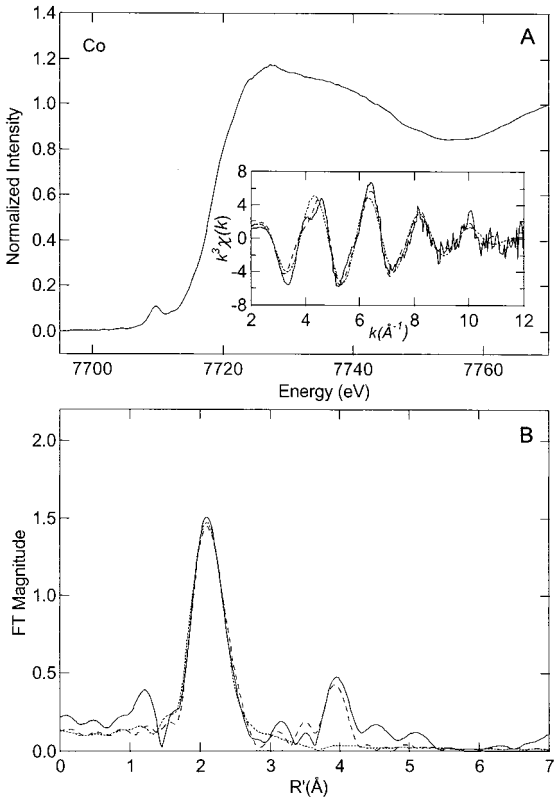

FIGURE 6: Co K-edge X-ray absorption spectrum for Co(II)−SmtB [1:1 Co(II):SmtB monomer] (A) and k^3-weighted EXAFS (A, inset) and Fourier transforms (B; $k = 2-12$ Å^{-1}) for Co(II)−SmtB (solid line) and theoretical EXAFS and FTs for Co−$S(O,N)_3$ (dotted line; fit 1, Table 3) and Zn−$S(imid)_2$(carboxylate) (dashed line; fit 2, Table 3).

shell Zn coordination environment that includes one sulfur and three light (oxygen or nitrogen) atoms (fit 1; Table 2), although based on goodness-of-fit criteria alone, the presence of two Cys thiolates in the first shell cannot be rigorously excluded.[2] The appearance in the Fourier transform (FT) of a strong 4 Å peak in the absence of a 3 Å peak is a unique fingerprint (Figure 5B). More typical is the coincident appearance of both a 3 Å and a 4 Å peak, which is diagnostic for imidazole (histidine) coordination (e.g., Figure 9B). In one other case, an archaeal zinc-containing ferredoxin (*24*), we have observed a 4 Å peak in the absence of a 3 Å peak, which in light of the crystal structure for this protein (*42*) was attributed to destructive interference between the 3 Å imidazole contribution and the EXAFS from a carboxylate ligand bound with a Zn−O−C angle of 126°. Application of a similar model to the EXAFS for Zn SmtB reveals a significant improvement in goodness-of-fit values when a carboxylate ligand is added to a histidine- and sulfur-containing Zn model (cf. fits 2 and 3; Table 2). The lower than expected Debye−Waller factors were also observed for the archaeal zinc-containing ferredoxins (*24*) and can be attributed to the destructive interference between the EXAFS contributions of the carboxylate and histidine ligands. Thus, the EXAFS for Zn SmtB are best fit assuming a Zn−$S(imid)_2$(carboxylate) coordination environment, with a Zn−O−C bond angle of approximately 126°. Fits assuming a Zn−O−C bond angle of 180° in Zn SmtB, the other common coordination geometry found in the PDB, do not model the destructive interference of the 3 Å peak as well (data not shown).

To provide a complementary probe of the coordination environment of the Co(II) complex formed by SmtB, XAS analysis of Co(II)-substituted SmtB was also performed (Figure 6). The position of the Co K-edge XAS spectrum (7718.3 eV first inflection) and the intensity of the 7710 eV preedge 1s→3d transition (0.14 eV) are indicative of Co(II) coordinated by mostly light atoms, with a total coordination number of 4 (*43*, *44*). The Co FT spectrum (Figure 6B) is qualitatively similar to that of the Zn FT spectrum (Figure 5B), including the strong 4 Å peak, indicating that Co(II) isomorphously replaces Zn(II). Detailed curve-fitting analysis of the Co EXAFS is again consistent with a first-shell coordination environment containing one sulfur and three light atoms (nitrogen, oxygen) (fit 1; Table 3). As with the Zn EXAFS, however, fits which incorporate two thiolate and two light-atom ligands give excellent goodness-of-fit values, but with larger metal−S Debye−Waller factors.[2] In coordination models which invoke a single thiolate ligand, these data are best fit with a scattering model which invokes destructive interference between a single carboxylate ligand and two imidazole (histidine) ligands (fit 2, Table 3). Taken together, these experiments provide compelling evidence that the Zn(II) and Co(II) coordination complexes in SmtB are identical.

Ni(II) Titrations of SmtB. Figure 7A shows the results of a representative titration of apo SmtB with Ni(II). The visible absorption spectrum is of very low intensity in the 550−800 nm region where d−d ligand field transitions of Ni(II) would be expected to occur ($\epsilon \leq 50$ M^{-1} cm^{-1}); in addition,

[2] VanZile, M., Cosper, N., Scott, R. A., and Giedroc, D. P., unpublished results.

Table 3: Curve-Fitting Results for Co EXAFS of SmtB[a]

sample filename (k range) $\Delta k^3\chi$	fit	shell	R_{as} (Å)	σ_{as}^2 (Å^2)	f'[b]
wt SmtB+Co	1	Co−N_3	1.97	0.0058	0.082
P2C2A (2−12 Å^{-1})		Co−S	2.23	0.0056	
$\Delta k^3\chi = 12.53$					
	2	Co−S	2.25	0.0035	0.068
		Co−N_2	1.99	0.0000	
		Co−C_2	2.90	0.0004	
		Co−C_2	[3.03]	[0.0004]	
		Co−C_2	[4.05]	[0.0005]	
		Co−N_2	[4.13]	[0.0005]	
		Co−O	1.86	0.0038	
		Co−C	[2.75]	[0.0056]	
		Co−O	[3.01]	[0.0061]	

[a] See footnotes to Table 2.

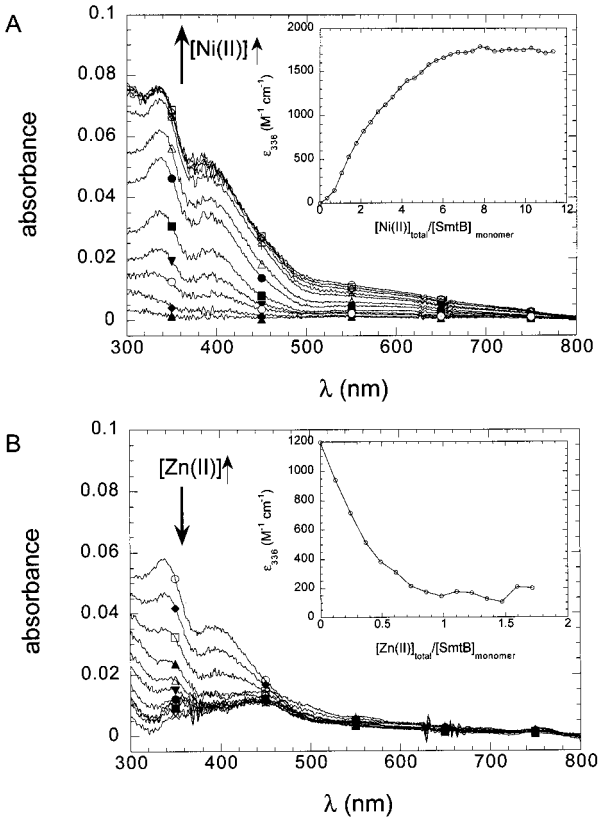

FIGURE 7: Ni(II) titrations of SmtB and subsequent displacement by added Zn(II). (A) Optical absorption spectra of 43.7 μM apo-SmtB titrated with increasing concentrations of Ni(II) in an aerobic environment. Inset: Ni(II) binding isotherm generated from the optical spectra plotted as ϵ_{336} vs total [Ni(II)]/total [SmtB monomer] ratio. (B) Changes in the optical absorption spectra of Ni(II)-substituted SmtB recorded in the presence of 4 molar equiv of Ni(II) following the addition of increasing amounts of Zn(II). Inset: Zn(II) displacement binding isotherm that results from analysis of the spectral data plotted as ϵ_{336} vs total [Zn(II)]/total [SmtB monomer] ratio. Conditions: pH 7.4, 0.15 M KCl, 22 °C.

there is some $S^- \rightarrow$Ni(II) LMCT absorption (300−500 nm region) with the peak maximum at 336 nm, suggestive of Ni(II)−thiolate coordination bonds but only at a large excess of Ni(II). Interestingly, when ϵ_{336} is plotted as a function of [Ni(II)]:[SmtB monomer] molar ratio, the isotherm is clearly sigmoidal, with comparatively little $S^- \rightarrow$Ni(II) LMCT absorption below a [Ni(II)]:[SmtB monomer] molar ratio of 1, and with maximal absorption in this region requiring ≈6 equiv of Ni(II) per SmtB monomer (at 48 μM monomer). However, stoichiometric Zn(II) (Figure 8B) and Co(II) (data not shown) readily dissociate Ni(II) from SmtB when incubated at a 4:1 stoichiometry, suggesting that Ni(II) binds in the same vicinity as Zn(II) and Co(II) on SmtB, but with a far lower affinity.

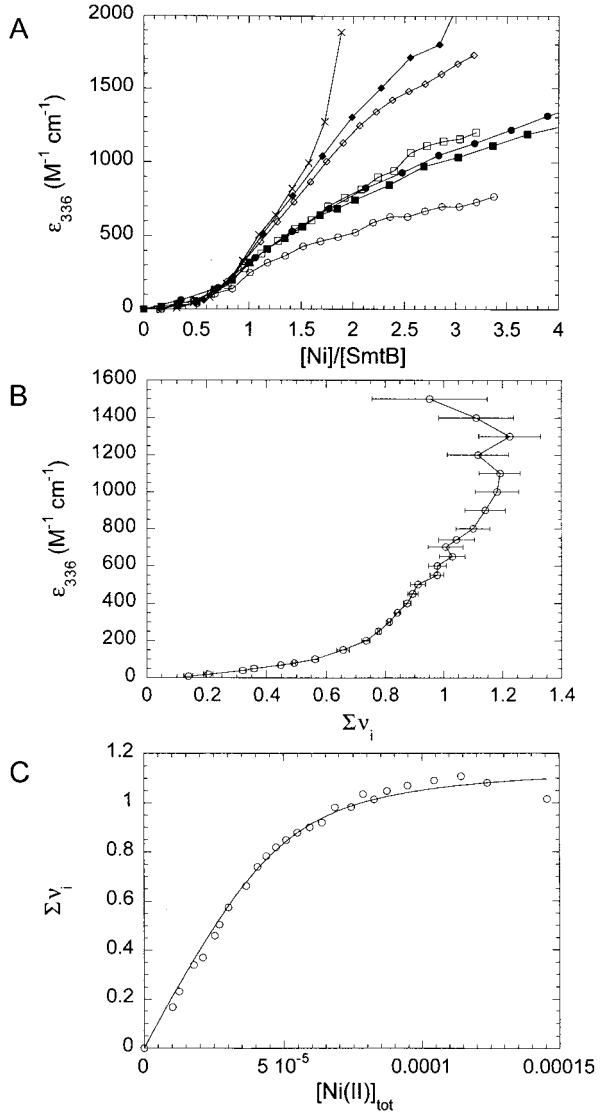

FIGURE 8: Ni(II) binding to apo-SmtB. (A) Series of Ni(II) binding curves plotted as molar absorptivity ϵ_{336} vs [Ni(II)]/[SmtB monomer] ratio recorded at 22 (○), 43.7 (■), 46.0 (●), 47.0 (□), 97 (◇), 109 (◆), and 197 (×) μM SmtB monomer. (B) Plot of the relationship of molar absorptivity (ϵ_{336}) vs $\Sigma\nu_i$ (see text for details). (C) Nonlinear least-squares fit of a model-independent Ni(II) binding isotherm (48 μM SmtB monomer) to a model corresponding to n identical sites characterized by an affinity K_{Ni}. Resolved parameters are $K_{Ni} = 1.7\ (\pm 0.4) \times 10^5\ M^{-1}$ and $n = 1.16\ (\pm 0.02)$.

Given the unusual shape of the binding isotherm (ϵ_{336} vs [Ni(II)]/[SmtB]), multiple titrations were carried out in which the SmtB monomer concentration was varied over a nearly 10-fold range, from 22 to 198 μM (Figure 8A). The binding curves which result essentially superimpose at [Ni(II)]/[SmtB] ≤0.5−0.6 and are characterized by very low detectable absorptivity, and ultimately diverge to greater ϵ_{336} values at lower [Ni(II)]/[SmtB] as the SmtB monomer concentration is raised. Application of a macromolecular binding density function analysis to this set of binding isotherms (*45*) allows a model-independent determination of $\Sigma\nu_i$, the average

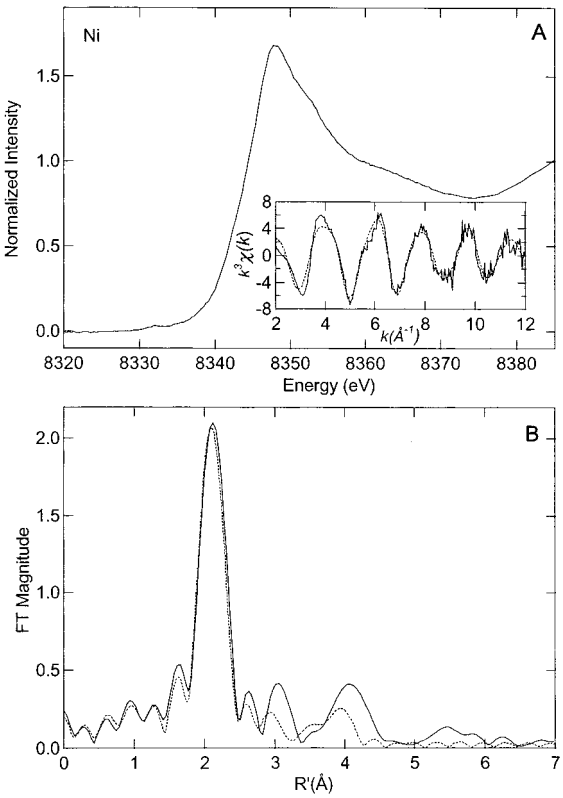

FIGURE 9: Ni K-edge X-ray absorption spectrum for $Ni_{0.8}$ SmtB (A) and k^3-weighted EXAFS (A, inset) and Fourier transforms (B) ($k = 2-12$ Å^{-1}) for $Ni_{0.8}$ SmtB monomer (solid line) and theoretical EXAFS and FTs for Ni−$(O,N)_4(imid)_2$ (dotted line; fit 5, Table 4).

number of Ni(II) ions bound per SmtB monomer [or more precisely, the distribution of Ni(II) ions bound in different states *i*], at each ϵ_{336} value. This plot is shown in Figure 8B and makes two important points. (1) The molar absorptivity at ϵ_{336} is *not* a simple linear function of the average degree of saturation of the SmtB monomer with Ni(II) ions. In fact, at most $\Sigma\nu_i$ values less than 1, there is little detectable absorptivity at 336 nm. (2) The maximum Ni(II) binding stoichiometry is near 1:1 even when ϵ_{336} is maximal ($\epsilon_{336} =$ 1700 M^{-1} cm^{-1} M^{-1}; see Figure 7A). Knowledge of the relationship between $\Sigma\nu_i$ and ϵ_{336} allows construction of a model-independent Ni(II) binding isotherm (Figure 8C; 48 μM protein monomer) which when fit to a 1:1 binding model allows resolution of $K_{Ni} = 1.7$ ($\pm$0.4) $\times$ 10^5 M^{-1} and $n =$ 1.16 ($\pm$0.02). A similar analysis of all model-independent Ni(II) binding isotherms reveals $K_{Ni} = 1.3$ ($\pm$0.5) $\times$ 10^5 M^{-1} and $n = 1.21$ ($\pm$0.04) or roughly 4 orders of magnitude less tightly than Co(II). These data suggest that at [Ni(II)]/[SmtB monomer] $\leq$0.6, Ni(II) forms a non-native metal complex which is likely not tetrahedral and largely lacks Ni(II)−thiolate bonds, perhaps drawing on ligands derived from each monomer; eventually, the metal complex ultimately rearranges to form a new 1:1 complex with at least one Ni(II)−thiolate bond, in a process that requires a significant molar excess of Ni(II).

A sample of Ni(II)-substituted SmtB was prepared at a [Ni(II)]:[SmtB monomer] ratio of 0.8 ($\Sigma\nu_i = 0.8$) and subjected to XAS analysis. The edge position and maximum intensity of the Ni K-edge XAS spectra (Figure 9A) as well as the intensity of the 8332 eV preedge peak are consistent

Table 4: Curve-Fitting Results for Ni EXAFS of SmtB ($\Sigma\nu_i =$ 0.80)[a]

sample filename (*k* range) $\Delta k^3\chi$	fit	shell	R_{as} (Å)	σ_{as}^2 (Å^2)	f'[b]
wt SmtB+ Ni	1	Ni−N_5	2.08	0.0026	0.086
P2N2A (2−12 Å^{-1})	2	Ni−N_6	2.08	0.0039	0.082
$\Delta k^3\chi = 13.99$	3	Ni−N_7	2.08	0.0052	0.083
	4	Ni−N_6	2.08	0.0039	0.076
		Ni−C	2.96	−0.0002	
		Ni−C	[3.07]	[−0.0002]	
		Ni−C	[4.09]	[−0.0003]	
		Ni−N	[4.15]	[−0.0003]	
	5	Ni−N_6	2.08	0.0039	0.077
		Ni−C_2	2.95	0.0038	
		Ni−C_2	[3.06]	[0.0038]	
		Ni−C_2	[4.08]	[0.0052]	
		Ni−N_2	[4.15]	[0.0054]	
	6	Ni−N_6	2.08	0.0039	0.080
		Ni−C_3	2.95	0.0072	
		Ni−C_3	[3.06]	[0.0072]	
		Ni−C_3	[4.07]	[0.0097]	
		Ni−N_3	[4.14]	[0.0100]	

[a] See footnotes to Table 2.

with a Ni(II) $(N,O)_6$ coordination environment (*46*). Furthermore, the Ni FT spectrum is characterized by typical metal−histidine interactions in which the second-shell 3 Å and 4 Å peaks are of comparable intensity (Figure 9B). Detailed curve-fitting analysis reveals that the average Ni(II) site is best fit with a model involving six light-atom scatterers (fit 2; Table 4), two of which result from imidazole (histidine) ligation (cf. fits 4−6; Table 4). This coordination geometry is expected to have extremely weak molar absorptivity throughout the visible region, as is observed (Figure 7). Thus, Ni(II) does not appear to have the same coordination environment as Co(II) or Zn(II) in SmtB.

DISCUSSION

The *smt* operon plays a key role in the resistance of *Synechococcus* bacterial strains to Zn(II), Cu(II), and Cd(II), and to a lesser extent by Co(II) and Ni(II) (*8*). The *smt* operon has been shown to be regulated by the transcriptional repressor SmtB which binds Zn(II) as determined by ^{65}Zn(II) equilibrium dialysis experiments (*9, 12*). Incubation of SmtB−DNA complexes with Zn(II) has been reported to reversibly inhibit DNA complex formation in the 50−100 μM range of Zn(II) concentration, as deduced from electrophoretic mobility shift assays (*9, 10*). These results are consistent with the hypothesis that the mechanism of derepression of the *smt* operon by Zn(II) involves simple Zn(II)-induced dissociation of the repressor, allowing for access by RNA polymerase and subsequent initiation of transcription. This simple hypothesis makes the prediction that the Zn(II) affinity will be appropriate such that regulation occurs in vivo over a concentration range of *free* metal ion comparable to $1/K_{Zn}$. Furthermore, it predicts that the ability of other divalent metals to induce the operon will be directly dictated by their relative affinities for the repressor (*3*). Many aspects of this hypothesis remain to be tested, including the mode of Zn(II) binding by SmtB. This report investigates the binding of Zn(II) to SmtB by determining the coordina-

tion environment and the affinity of the metal binding site and begins to define the metal specificity of SmtB.

Our experiments show that SmtB binds Zn(II), Co(II), and Ni(II), each with a stoichiometry of 1 metal ion per SmtB monomer. Optical absorption spectra of the Co(II) complex and Zn and Co EXAFS studies reveal that Zn(II) and Co(II) occupy the same binding site to form a tetrahedral, or distorted tetrahedral, coordination environment that appears to contain one cysteine thiolate ligand in the first shell, in the presence of a mixture of carboxylate- and imidazole-containing ligands. Co(II) binds with K_{Co} of 1.7×10^9 M^{-1}, while Zn(II) binds with an apparent affinity in the $10^{11}-10^{12}$ M^{-1} range under these conditions. It is interesting to note that K_{Zn} and K_{Co} determined for SmtB are essentially identical to those determined for the structural Zn(II) site in phage T4 gene 32 protein under very similar solution conditions (*17*). Ni(II) binds to SmtB with a far lower apparent affinity than Co(II), $K_{Ni} = 1.3 \times 10^5$ M^{-1}, and exhibits complex binding equilibria characterized by the formation of a non-native octahedral or distorted octahedral site largely lacking cysteine ligands, which ultimately rearranges to form an average site of lower coordination number (given the low but significant absorption in the d−d ligand field transition region) with some Ni(II)−thiolate character (*31*). Given that apo SmtB is largely a dimer under these conditions, it seems possible that the first Ni(II) ion binds to the dimer in a non-native geometry, perhaps across the dimer interface, but is nearby or perhaps shares a subset of ligands with the native site on each monomer; as the second Ni(II) binds to the dimer, it recruits a cysteine ligand, ultimately perturbing the original complex with no change in the average number of Ni(II) ions bound ($\Sigma\nu_i$). Further evidence that the stoichiometry remains 1:1 under all conditions greater than stoichiometric Ni(II) is that 1 equiv of Zn(II) results in full displacement of the bound Ni(II). We have previously observed complex metal binding equilibria like these in a Co(II) titration of a metal ligand mutant of the S_3N Zn(II) site of T4 gene 32 protein (*47*), where the optical data suggested that formation of an octahedral complex containing little thiolate character was followed by rearrangement to a tetrahedral or pentacoordinate complex in the presence of excess Co(II) (*17*).

This Zn(II) stoichiometry and affinity determined by our optical titrations at first glance contradicts a published ^{65}Zn equilibrium dialysis experiment which concluded that Zn(II) binds to SmtB with a 2:1 Zn(II)/monomer stoichiometry, modeled as two independent binding events with a stepwise affinity constant of only 3×10^5 M^{-1} (K_d of 3.5×10^{-6} M) (*12*). However, in that experiment, the high-affinity zinc chelator nitrilotriacetic acid (NTA, $K_{Zn} = 1.8 \times 10^8$ M^{-1} at pH 7.4, 0.1 M NaCl, 25 °C) was present in large excess (1 mM) over SmtB monomer concentration (37.5 μM) on *both* sides of the dialysis membrane, with all of the added ^{65}Zn present only on the non-protein-containing side of the dialysis membrane at the start of the experiment. Thus, the ^{65}Zn will equilibrate across the membrane in a way which is dictated by K_{Zn} for NTA vs SmtB. The fact that there was significantly more ^{65}Zn on the SmtB-containing side of the membrane at equilibrium is direct evidence that K_{Zn} for SmtB $\gg K_{Zn}$ for NTA. A reanalysis of the data presented in (*12*) reveals essentially stoichiometric 1:1 binding of zinc to SmtB with an affinity too tight to measure under those solution conditions, $K_{Zn} \gg 10^9$ M^{-1} (data not shown). This is fully consistent with the findings presented here.

If a second Zn(II) binding site is indeed present on SmtB, we conservatively estimate that its affinity would have to be less than 10^5 M^{-1}, since anything tighter would have effectively competed with mag-fura-2 (Figures 2 and 3). In all of these experiments, once all of the SmtB binding sites in solution are loaded with Zn(II), a single mole equivalent of Zn(II) relative to [mag-fura-2] is all that is required to fully saturate the competitor ligand. UV−vis Co(II) titrations carried out at high concentrations of protein (≥300 μM) also provide no evidence for a second Co(II) binding site. Thus, if one is present, it would have to be bound in an octahedral liganding geometry with $K_{Co} \leq 10^4$ M^{-1}, in a way which is not easily distinguished from hexa-aquo Co(II). Whether or not the closely related *Synechocystis* ZiaR, like SmtB, contains only one high-affinity Zn(II) binding site is as yet unclear. Preliminary mag-fura-2 competition experiments reveal that ZiaR, like SmtB, contains one-high affinity Zn(II) site, with $K_{Zn} \geq 10^{11}$ M^{-1}; Zn EXAFS studies suggest that this site is spectroscopically similar to that in SmtB.[3] However, metal binding experiments with ZiaR are complicated by the fact that all preparations of the protein reproducibly contain less than the full complement of reduced cysteine residues.[3]

Other factors regarding the structure and stability of SmtB may also significantly complicate the analysis of other metal and DNA binding data in the literature. We were careful to perform our optical titration experiments with fully reduced apoprotein in the absence of exogenous thiols (such as DTT) in an anaerobic environment. We have found that the three cysteines of SmtB remain reduced and air-stable for ≥8 h at room temperature as quantitated by DTNB reactivity time course experiments; however, we have also found that SmtB, like other members of the ArsR family of proteins, is capable of forming cross-linked dimers even when frozen at −80 °C for a few months in the absence of reducing agent (data not shown). Furthermore, we have experienced difficulties in removing all of the EDTA from SmtB purified in the presence of this chelator as is typically done; an exhaustive 2 day dialysis with multiple changes of buffer is required to fully remove adventitiously bound EDTA.[4] Obviously, the presence of bound chelator will severely complicate the interpretation of metal binding experiments. Finally, in our hands, the addition of excess Zn(II) at concentrations of protein in the low micromolar range results in precipitation of the protein under most solution conditions (data not shown). Thus, it seems possible that Zn(II)-induced dissociation of SmtB from the DNA observed by others in electrophoretic mobility shift experiments (*9*, *10*) may at least partially derive from precipitation of the protein.

The optical absorption and EXAFS data show that the first shell of coordinating ligands contains one to two cysteine thiolate ligands which must be derived from the three Cys in SmtB: Cys14 in the unstructured N-terminal arm; Cys61 just N-terminal to the putative helix−turn−helix DNA binding motif; or Cys121 near the C-terminus (*14*). Of these, only Cys61 is strongly conserved among SmtB, ZiaR, and

[3] Busenlehner, L., Cosper, N., Scott, R. A., and Giedroc, D. P., unpublished results.

[4] VanZile, M., and Giedroc, D. P., unpublished results.

CadC (as well as ArsR) (*48*). Cys14 is somewhat conserved in the Zn/Cd-specific metalloregulatory repressors even though the sequences and lengths of the N-terminal domains diverge rather strongly from one another, and at least in one case, *S. aureus* 912 CzrA (ZntA) (*49*), is absent altogether. Interestingly, none of the conserved cysteines in SmtB have been reported to be absolutely essential for Zn(II) induction in vivo (*15*). However, an SmtB mutant containing a T11S/C14S substitution, although Zn(II)-inducible, appeared to be less so than the wild-type protein (*15*). These functional data suggest that Cys14 is a strong candidate for providing a thiolate ligand in SmtB. This would be consistent with a recent NMR study which suggests that only the backbone amide group of Cys14 and immediately adjacent residues are strongly perturbed in solution upon addition of Zn(II) to apo-SmtB (*16*, *50*). These experiments suggest that there might be a conformational change in the protein which occurs upon Zn(II) binding to the high-affinity site; this in turn might modulate the affinity of SmtB for the DNA.

The extent to which the binding of Zn(II), Co(II), or Ni(II) to the metal site characterized here modulates the affinity of SmtB for DNA or otherwise alters the initiation of transcription from the *smt* operator−promoter region is not yet known. Two limiting possibilities exist, however. One is that this high-affinity metal site plays no role in regulation, but instead plays a structural role in stabilizing the protein against thermal or other denaturation, or simply stabilizes the dimeric form of the repressor. Previous analytical ultracentrifugation experiments do indeed suggest that Zn(II) stabilizes the SmtB homodimer (*12*). This scenario might be plausible if two metal binding sites with very different binding affinities do indeed exist on SmtB. Here, the high-affinity site would play a structural role, while a lower affinity site might play an allosteric or regulatory role. However, since only one Zn(II) binding site is identified in our experiments, this possibility is unlikely. We propose that this high-affinity Zn(II) site is indeed regulatory, and binding here allosterically modulates DNA binding affinity and/or structure of the *smt* operator−promoter region in a way which allows for the initiation of transcription. If this is the case, our characterization of this high-affinity zinc site has significant consequences for the fundamental features of zinc metalloregulation in vivo, since in order for this site on SmtB to perform a metalloregulatory switch function, free zinc pools in *Synechococcus* would have to vary over the picomolar concentration range, not in the micromolar range as might have been anticipated. SmtA, the cyanobacterial metallothionein whose expression is regulated by Zn(II)-SmtB, is known to have a high affinity for Zn(II) which may be at least partially responsible for maintaining very low intracellular free zinc concentrations in *Synechococcus* (*7*). It will be interesting to determine if SmtA is capable of facile removal of Zn(II) from SmtB.

The free concentration of zinc inside bacterial or mammalian cells under resting or zinc-stimulated conditions is not known with certainty, due principally to the lack of chromophoric dyes which are characterized by zinc affinities in the picomolar to nanomolar range and are specific enough for Zn(II) to function in an in vivo milieu. Significant progress has recently been made in this area, however (*19*, *51*). For example, total Zn(II) concentrations in the low micromolar range outside of cyanobacterial cells are known to be required to derepress the SmtB-mediated repression of the *smt* operator−promoter region; however, it is not known how these changes in *total* Zn(II) translate into changes in *free* Zn(II) concentration inside cells or within particular cellular compartments. If the free concentration of Zn(II) is vanishingly small in the resting state, and only changes slightly upon stimulation, activation of SmtB by zinc to mediate zinc homeostasis in *Synechococcus* might have interesting parallels to copper homeostasis in prokaryotic and eukaryotic cells, in which specific copper chaperones are required to insert copper ions into copper enzymes under conditions of essentially no free Cu in the cell (for a review, see ref *52*). Experiments are currently underway to further define the mechanism by which Zn(II) induces this metalloregulatory system.

ACKNOWLEDGMENT

We thank Dr. Leo Hall of the University of Alabama−Birmingham for his generous gift of plasmid pSRK15-1 and an initial preparation of purified SmtB. XAS data were collected at SSRL, which is operated by the Department of Energy, Division of Chemical Sciences. The SSRL Laboratory is supported by the NIH, Biomedical Resource Technology Program, Division of Research Resources.

REFERENCES

1. Coleman, J. E. (1992) *Annu. Rev. Biochem. 61*, 897−946.
2. Vallee, B. L., and Fallchuk, K. H. (1993) *Physiol. Rev. 73*, 79−118.
3. O'Halloran, T. V. (1989) in *Metal Ions in Biological Systems. Vol. 25. Interrelations among Metal Ions, Enzymes, and Gene Expression* (Sigel, H., and Sigel, A., Eds.) pp 105−146, Marcel Dekker, Inc., New York and Basel.
4. O'Halloran, T. V. (1993) *Science 261*, 715−725.
5. Shi, W., Wu, J., and Rosen, B. P. (1994) *J. Biol. Chem. 269*, 19826−19829.
6. Robinson, N. J., Bird, A. J., and Turner, J. S. (1998) in *Metal ions in Gene Regulation* (Silver, S., and Walden, W., Eds.) pp 372−397, Chapman and Hall, New York.
7. Daniels, M. J., Turner-Cavet, J. S., Selkirk, R., Sun, H., Parkinson, J. A., Sadler, P. J., and Robinson, N. J. (1998) *J. Biol. Chem. 273*, 22957−22961.
8. Huckle, J. W., Morby, A. P., Turner, J. S., and Robinson, N. J. (1993) *Mol. Microbiol. 7*, 177−187.
9. Erbe, J. L., Taylor, K. B., and Hall, L. M. (1995) *Nucleic Acids Res. 23*, 2472−2478.
10. Morby, A. P., Turner, J. S., Huckle, J. W., and Robinson, N. J. (1993) *Nucleic Acids Res. 21*, 921−925.
11. Thelwell, C., Robinson, N. J., and Turner-Cavet, J. S. (1998) *Proc. Natl. Acad. Sci. U.S.A. 95*, 10728−10733.
12. Kar, S. R., Adams, A. C., Lebowitz, J., Taylor, K. B., and Hall, L. M. (1997) *Biochemistry 36*, 15343−15348.
13. Rosen, B. P. (1996) *J. Biol. Inorg. Chem. 1*, 273−277.
14. Cook, W. J., Kar, S. R., Taylor, K. B., and Hall, L. M. (1998) *J. Mol. Biol. 275*, 337−346.
15. Turner, J. S., Glands, P. D., Samson, A. C. R., and Robinson, N. J. (1996) *Nucleic Acids Res. 19*, 3714−3721.
16. Kosada, T., Morita, E. H., Miura, A., Yamazaki, T., Hayashi, H., and Kyogoku, Y. (1999) *J. Biomol. NMR 14*, 191−192.
17. Guo, J., and Giedroc, D. P. (1997) *Biochemistry 36*, 730−742.
18. Pace, C. N., Vajdos, F., Fee, L., Grimsley, G., and Gray, T. (1995) *Protein Sci. 4*, 2411−2423.
19. Fahrni, C. J., and O'Halloran, T. V. (1999) *J. Am. Chem. Soc. 121*, 11448−11458.
20. Walkup, G. K., and Imperiali, B. (1997) *J. Am. Chem. Soc. 119*, 3443−3450.

21. Jefferson, J. R., Hunt, J. B., and Ginsburg, A. (1990) *Anal. Biochem. 187*, 328−336.
22. Scott, R. A. (1985) *Methods Enzymol. 117*, 414−458.
23. Yamaguchi, K., Cosper, N. J., Stalhandske, C. M. V., Scott, R. A., Pearson, M. A., Karplus, P. A., and Hausinger, R. P. (1999) *J. Biol. Inorg. Chem. 4*, 468−477.
24. Cosper, N. J., Stahlhandske, C. M. V., Iwasaki, H., Oshima, T., Scott, R. A., and Iwasaki, T. (1999) *J. Biol. Chem. 274*, 23160−23168.
25. Zabinsky, S. I., Rehr, J. J., Ankudinov, A., Albers, R. C., and Elber, M. J. (1995) *Phys. Rev. B 52*, 2995−3009.
26. Horrocks, W. D., Ishley, J. N., Holmquist, B., and Thompson, J. S. (1980) *J. Inorg. Biochem. 12*, 131−141.
27. Bear, C. A., Duggen, K. A., and Freeman, H. C. (1975) *Acta Crystallogr., Sect. B 31*, 2713−2715.
28. Konopelski, J. P., Reimann, C. W., Hubbard, C. R., Mighell, A. D., and Santoro, A. (1976) *Acta Crystallogr., Sect. B 32*, 2911−2913.
29. Strandberg, R., and Lundberg, K. S. (1971) *Acta Chem. Scand. 25*, 1767−1774.
30. Giedroc, D. P., Keating, K. M., Williams, K. R., Konigsberg, W. H., and Coleman, J. E. (1986) *Proc. Natl. Acad. Sci. U.S.A. 83*, 8452−8456.
31. Chen, X., Chu, M., and Giedroc, D. P. (2000) *J. Biol. Inorg. Chem. 5*, 93−101.
32. Vasak, M., Kägi, H. H. R., Holmquist, B., and Vallee, B. L. (1981) *Biochemistry 20*, 6659−6664.
33. May, S. W., and Kuo, J.-Y. (1978) *Biochemistry 17*, 3333−3338.
34. Guo, J., Wang, S., Dong, J., Qiu, H., Scott, R. A., and Giedroc, D. P. (1995) *J. Am. Chem. Soc. 117*, 9437−9440.
35. Krizek, B. A., Merkle, D. L., and Berg, J. M. (1993) *Inorg. Chem. 32*, 937−940.
36. Krizek, B. A., Amann, B. T., Kilfoil, V. J., Merkle, D. L., and Berg, J. M. (1991) *J. Am. Chem. Soc. 113*, 4518−4523.
37. Mely, Y., Cornille, F., Fournié-Zaluski, M.-C., Darlix, J.-L., Roques, B. P., and Gérard, D. (1991) *Biopolymers 31*, 899−906.
38. Berg, J. M., and Merkle, D. L. (1989) *J. Am. Chem. Soc. 111*, 3759−3761.
39. Hunt, J. B., Neece, S. H., and Ginsburg, A. (1985) *Anal. Biochem. 146*, 150−157.
40. Jacquemet, L., Aberdam, D., Adrait, A., Hazemann, J.-L., Latour, J.-M., and Michaud-Soret, I. (1998) *Biochemistry 37*, 2564−2571.
41. Clark-Baldwin, K., Tierney, D. L., Govindaswamy, N., Gruff, E. S., Kim, C., Berg, J., Koch, S. A., and Penner-Hahn, J. E. (1998) *J. Am. Chem. Soc. 120*, 8401−8409.
42. Fujii, T., Hata, Y., Wagaki, T., Tanaka, N., and Oshima, T. (1996) *Nat. Struct. Biol. 3*, 834−837.
43. Scheuring, E. M., Sagi, I., and Chance, M. R. (1994) *Biochemistry 33*, 6310−6315.
44. Zhang, J.-H., Kurtz, D. M., Maroney, M. J., and Whitehead, J. P. (1992) *Inorg. Chem. 31*, 1359−1366.
45. Lohman, T. M., and Bujalowski, W. (1991) *Methods Enzymol. 208*, 258−290.
46. Colpas, G. J., Maroney, M. J., Bagyinka, C., Kumar, M., Willis, W. S., Suib, S. L., Baidya, N., and Mascharak, P. K. (1991) *Inorg. Chem. 30*, 920−928.
47. Qiu, H., and Giedroc, D. P. (1994) *Biochemistry 33*, 8139−8148.
48. Wu, J., and Rosen, B. P. (1993) *J. Biol. Chem. 268*, 52−58.
49. Makoto, K., Hideo, H., and Toshiko, O. (1999) *Microbiol. Immunol. 43*, 115−125.
50. Morita, E. H., Kosada, T., Yamazaki, T., Kyogoku, Y., and Hayashi, H. (1998) *J. Biomol. NMR 12*, 453−454.
51. Nasir, M. S., Fahrni, C. J., Suhy, D. A., Kolodsick, K. J., Singer, C. P., and O'Halloran, T. V. (1999) *J. Biol. Inorg. Chem. 4*, 775−783.
52. Rosenzweig, A. C., and O'Halloran, T. V. (2000) *Curr. Opin. Chem. Biol. 4*, 140−147.
53. Kuzmic, P. (1996) *Anal. Biochem. 237*, 260−273.

BI001140O